

**Predictions of MESSENGER Neutron Spectrometer Measurements for Mercury's Polar Regions.** David J. Lawrence<sup>1</sup>, John K. Harmon<sup>2</sup>, William C. Feldman<sup>3</sup>, David A. Paige<sup>4</sup>, Patrick N. Peplowski<sup>1</sup>, Edgar A. Rhodes<sup>1</sup>, Christina M. Selby<sup>1</sup>, Sean C. Solomon<sup>5</sup>; <sup>1</sup>Johns Hopkins University Applied Physics Laboratory (11100 Johns Hopkins Drive, Laurel, MD, 20723; David.J.Lawrence@jhuapl.edu); <sup>2</sup>Arecibo Observatory, Arecibo PR 00612; <sup>3</sup>Planetary Science Institute, Tucson, AZ 85719; <sup>4</sup>University of California Los Angeles, Los Angeles, CA 90095 <sup>5</sup>Carnegie Institution of Washington, Washington, DC 20015.

**Introduction:** Earth-based radar measurements of Mercury's poles suggest that large amounts of water ice may be present near each pole [1]. The existence of this water ice can be explained by the fact that Mercury's rotation axis is nearly perpendicular to its orbital plane so that portions of the floors of near-polar craters are in permanent shadow and are therefore sufficiently cold to trap externally delivered water and other volatiles as ices over geologically long time periods. One of the goals of the MESSENGER mission to Mercury is to use planetary neutron spectroscopy to detect and measure hydrogen abundances associated with these polar deposits.

From five years of Arecibo S-band radar data, Harmon et al. [1] produced the most complete maps of radar reflectivity that indicate the likely locations of water ice at both Mercury poles. These data, combined with recent Mercury flyby data from and models for the MESSENGER Neutron Spectrometer (NS) [2], allow us for the first time to make detailed, quantitative predictions of the neutron counting rates that might be returned by the NS after MESSENGER goes into orbit about Mercury in March 2011. This study presents predicted neutron counting rates for three different possible Mercury polar water ice abundances.

**Arecibo Radar Data:** Dimensionless radar reflectivity (from Fig. 3b of [1]) mapped onto  $1/8^\circ \times 1/8^\circ$  pixels (expressed as radar cross section per unit surface area) of Mercury's north polar region is shown in Fig. 1. All signals greater than four standard deviations ( $4\sigma$ ) of the noise are regarded as consistent with surface or near-surface expressions of water ice [1]. A number of craters show large areas of enhanced radar reflectivity, as do several intercrater regions. The dashed white line in Fig. 1 shows the expected full-width, half-maximum (FWHM) spatial footprint of the NS for a 200-km spacecraft altitude, which is MESSENGER's lowest periapsis altitude. Because of this large footprint, individual craters will not be resolved with NS data. However, if the water ice abundances are as large as suggested [1], then as is shown below, a measurable hydrogen signal should be detectable with NS data. In addition, lunar surface temperature data [3] show that the Moon's polar cold traps are more extensive than previously thought because they are surrounded by regions in which water ice can be stable

tens of cm below the surface. If such near-surface "permafrost" regions are present on Mercury, then the NS signal may be larger than assumed here, since epithermal neutrons are sensitive to depths of tens of cm.

**Neutron Forward Model:** Our prediction of the NS signal uses a forward modeling process similar to that validated with planetary gamma-ray data [4]. A "model" abundance distribution at high spatial resolution is derived from available data. This distribution is converted to a measurable counting rate using known physics processes. The high-spatial-resolution model map is converted to a simulated orbital measurement with a calculated spatial response. Uncertainties from Poisson counting statistics are applied to create a predicted neutron map.

For Mercury, the modeled hydrogen abundance distribution is obtained from Arecibo radar data. All  $1/8^\circ \times 1/8^\circ$  pixels with signals  $>4\sigma$  are assigned a positive hydrogen concentration [1] and converted to a neutron counting rate associated with a given hydrogen concentration and hydrogen-free soil overburden. We investigate three scenarios: (1) 100 wt.% water ice at the surface in all areas of high radar reflectivity. This is the large-abundance end-member and results in the largest neutron signal. (2) 100 wt.% water ice covered with 20 cm of dry regolith in all areas of high radar reflectivity. This case is being considered because multiwavelength radar studies suggest that the polar deposits may be covered by 10–20 cm thickness of dry material [1]. (3) 50 wt.% water ice at the surface in all areas of high radar reflectivity. This lower-abundance case stretches the limits of detectability with NS data.

The neutron counting rates for each scenario are determined from model calculations validated with the measured NS flyby data. Specifically, we use a neutron counting rate of 10 counts per second (cps), the maximum rate measured during the MESSENGER flybys. From calculations with the particle transport code MCNPX [5], surface neutron counting rates for the three scenarios are 0.034, 0.09, and 0.2 cps. To simplify the later calculations, the  $1/8^\circ \times 1/8^\circ$  pixels are rebinned to  $0.5^\circ \times 0.5^\circ$  pixels, which are the standard base-map pixels for planetary nuclear spectroscopy studies [6]. Figure 2 shows the resulting counting rate map for case 1, given in counts per 20 s, because 20 s is the planned time cadence for NS measurements.

Spatial smoothing is carried out using calculated spatial response functions for planetary nuclear spectroscopy [7,8]. The FWHM of the spatial response is linearly dependent on spacecraft altitude and scales as  $1.5 \times \text{altitude}$ . A new altitude-dependent code for equal-area, spherical smoothing was implemented to account for the large altitude variations in the elliptical orbit.

**Results and Discussion:** The result of smoothing the modeled maps of Fig. 2 is shown in Fig. 3. This map represents the best-case measurement with no statistical or systematic uncertainties. The circular gap centered on the pole reflects the fact that MESSENGER's orbital inclination will not exceed  $85^\circ$ , so there will be no sub-spacecraft measurements poleward of such a latitude. Although no individual craters are resolved, the model hydrogen distribution creates a signal that is 4.1% lower than the counting rate for dry material. For comparison, the maximum signal magnitudes for cases 2 and 3 are 3.9% and 3.4%, below that for dry soil, respectively. For reference, this magnitude of signal is about two-thirds that measured for Cabaeus crater near the lunar south pole by the Lunar Prospector NS [9].

The extent to which these signals can be detected depends critically on the expected measurement uncertainties. Figure 4 shows the lower-limit uncertainties from Poisson counting statistics, now mapped onto

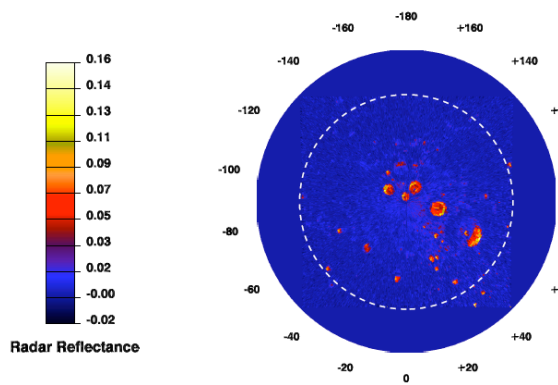


**Figure 1.** Mercury radar reflectivity, poleward of  $80^\circ\text{N}$  [1]. The dashed white line shows the NS footprint (at FWHM) for a spacecraft altitude of 200 km.

$200 \times 200 \text{ km}^2$  quasi-equal-area pixels. These uncertainties are for a one-year nominal MESSENGER mission, an 85% duty cycle [5], and altitude-dependent corrections to the total counts. With no other systematic uncertainties, signal-to-background detections of  $11\text{-}\sigma$ ,  $10\text{-}\sigma$ , and  $9\text{-}\sigma$  can be achieved on  $200 \times 200 \text{ km}^2$  pixels for each of the three cases. Detections with higher significance could be made for longitudinally averaged data. However, given the highly asymmetric orbit and the models that are required to correct the systematic variations in the neutron data [2], we expect that the overall systematic uncertainties will be no better than 0.5–1%. In such a case, detections of 4- to  $8\text{-}\sigma$  signals are still achievable.

**References:** [1] J.K. Harmon et al., *Icarus*, in press, 2011; [2] D.J. Lawrence et al., *Icarus*, 209, 195, 2010; [3] D.A. Paige et al., *Science*, 330, 479, 2010; [4] J.J. Hagerty et al., *JGR*, 111, 10.1029/2005JE002592, 2006; [5] D.J. Lawrence et al., *JGR*, 111, 10.1029/2005JE002637, 2006; [6] D.J. Lawrence et al., *JGR*, 109, 10.1029/2003JE002206, 2004; [7] D.J. Lawrence et al., *JGR*, 108, 10.1029/2003JE002050, 2003; [8] S. Maurice et al., *JGR*, 109, 10.1029/2003JE002208, 2004; [9] W.C. Feldman et al., *JGR*, 107, 23231, 2001.

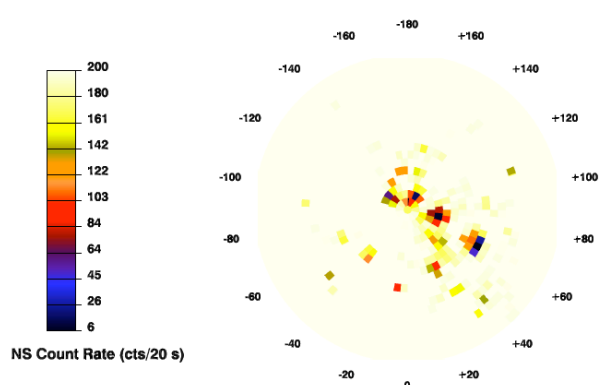


**Figure 2.** High spatial resolution model NS counting rates, poleward of  $80^\circ\text{N}$ , binned to  $0.5^\circ \times 0.5^\circ$  pixels under the assumption that areas of high radar reflectivity have 100 wt.%  $\text{H}_2\text{O}$  at the surface.

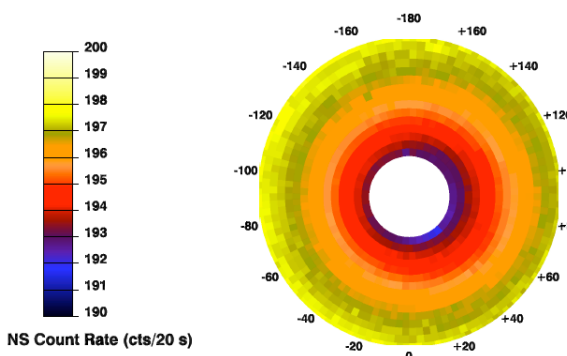


**Figure 3.** Simulated NS counting rate as propagated through the NS spatial response. This map shows all values poleward of  $70^\circ\text{N}$  with no statistical or systematic uncertainties.

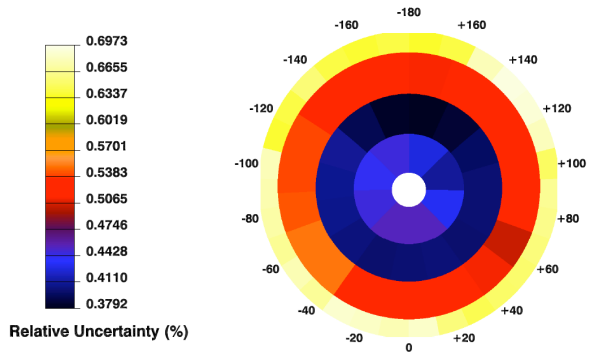


**Figure 4.** Expected uncertainties, poleward of  $70^\circ\text{N}$ , from Poisson counting statistics for a one-year MESSENGER mission. Pixels are approximately  $200 \text{ km} \times 200 \text{ km}$ .